Chapter 4

Segmentation of Water Body and Lakeshore Changes behind an Island Owing to Wind Waves

Takaaki Uda, Masumi Serizawa and Shiho Miyahara

Additional information is available at the end of the chapter

http://dx.doi.org/10.5772/intechopen.72550

Abstract

In a slender water body with a large aspect ratio, the angle of wind waves relative to the direction normal to the shoreline may exceed 45°, resulting in the emergence of cuspate forelands and the segmentation of the water body. The BG model was used to predict the segmentation of a rectangular water body by wind waves when the probability of occurrence of the wind direction is given by a circular or elliptic distribution, and the segmentation of a rectangular water body into a circular or elliptic lake was predicted in each case. The segmentation of a shallow water body with a triangular or crescent shape was also predicted together with the prediction of lakeshore changes when a rocky or sandy island exists in a circular lake.

Keywords: closed water body, wind waves, segmentation, lakeshore changes, BG model, cuspate foreland, island

1. Introduction

In a shallow water body, beach changes may take place owing to wind waves. In a narrow water body with a large aspect ratio, the angle of wind waves relative to the direction normal to the shoreline may exceed 45°, and the shoreline may become unstable because the fetch distance in the direction of the principal axis of the water body is sufficiently large for waves with significant energy to be generated [1, 2]. Therefore, cuspate forelands that develop from both shores of a narrow water body connect with each other, resulting in the segmentation of the water body into smaller rounded lakes [3, 4]. For example, **Figure 1** shows the segmentation of a lagoon facing the Chukchi Sea in Russia [3, 4]. In this example, five elliptic lakes can be observed as a result of segmentation, and their axes are parallel to each other. **Figure 2** shows an enlarged satellite image of the rectangular area in **Figure 1**, and in this image, lake segmentation at a primitive

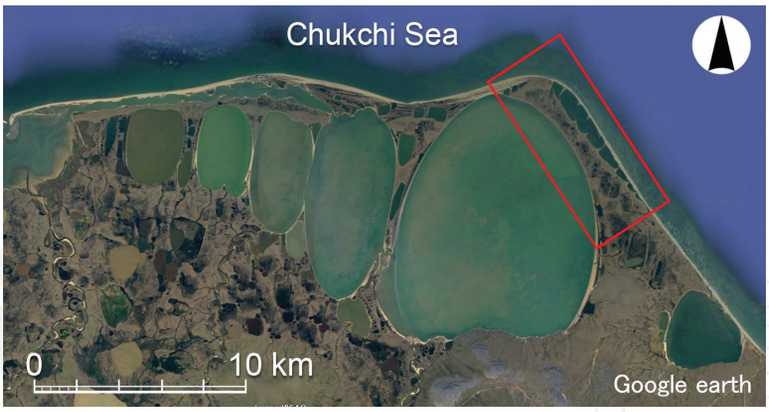

Figure 1. Example of segmentation of slender water body: Lagoons facing Chukchi Sea [3, 4].

stage can be seen with the alternate development of cuspate forelands. Regarding these phenomena, the division and reduction of the fetch distance owing to the formation of a large shoreline protrusion associated with shoreline instability under high-wave-angle conditions and the resulting change in the wave field are key factors. Ashton et al. [4] predicted that the forelands formed along the shoreline connect with each other, resulting in the segmentation of the water body into smaller rounded lakes. Uda et al. [5] predicted the three-dimensional (3-D) segmentation of a shallow rectangular water body using the BG model (a model for predicting 3-D beach changes based on Bagnold's concept) [6]. Uda et al. studied the emergence and mergence of small lakes and their segmentation using the same model [7], assuming that the wind blew from all directions between 0 and 360° with the same probability of occurrence and intensity, that is, a circular distribution of the probability. The segmentation into elliptic shapes, as shown in **Figure 1**, was not predicted in their study. It may be accomplished, assuming that the probability of occurrence of the wind direction is given by an elliptic distribution, similarly to the case of oriented lakes [8]. In this study, the segmentation of a rectangular water body was predicted, given a circular or elliptic distribution of the probability of occurrence of the wind direction.

In the coastal area, the segmentation of a shallow water body with a triangular or crescent shape can also be observed. To study the mechanism of segmentation of such a water body, several examples of segmentation together with the development of sand spits along the lakeshore were examined in Lagoa de Mangueira in Brazil, Lake Saroma and Lake Kitaura in

Figure 2. Enlarged satellite image of rectangular area in **Figure 1**.

Japan. Then, the BG model was used to investigate the segmentation of a shallow water body with a triangular or crescent shape, and 3-D beach changes during the segmentation of a shallow water body into small lakes were predicted.

When wind waves are incident to the lakeshore in a closed water body with a rocky or sandy island, topographic changes may occur on the lee of the island because of the wave-sheltering effect. Since a rocky island is fixed at a location in a closed water body, the wave-sheltering effect of the island is constant with time, and the lakeshore converges to a certain stable form after the wave action for a sufficiently long time. When a sandy island is located in a closed water body, however, the island itself can deform owing to the action of wind waves, resulting in the successive change in wave field. Thus, more complicated lakeshore changes will occur. Here, Lake Balkhash located in Kazakhstan [9] was selected as an example, and the BG model was used for predicting lakeshore changes when a rocky or sandy island exists in a circular lake.

2. Examples of cuspate forelands in lake

2.1. Lakeshore in Lagoa de Mangueira

Figure 3 shows an example of segmentation and the development of sand spits along the lakeshore of Lagoa de Mangueira (location: 33°09′59″S, 52°49′32″W) in Brazil [7]. The crescent lake is 100 km long and 10 km wide at the center of the lake. Many cuspate forelands have developed along the lakeshore and, in particular, the intervals of the cuspate forelands formed on the west shore become short near the south end of the lake. On the other hand, sand spits with similar shapes and cuspate forelands have developed along the east and west shores, respectively, in the north part of the lake. This is a typical example of segmentation and the development of sand spits in a crescent lake.

2.2. Lakeshore in Lake Saroma

Figure 4 shows a satellite image of an abandoned inlet located at the east end of Lake Saroma in Hokkaido, Japan (Location: 44°08′03″N, 143°59′04″E) [10]. This water body has a triangular shape, and segmentation of a water body can be seen near the east end. When enlarging the rectangular area in the satellite image of **Figures 4** and **5** is obtained. For the wind rose in Lake Saroma, the predominant wind direction is WNW, resulting in the eastward development of sand spits. On the south shore is Tofutsu fishing port, as shown in **Figure 5**. East of

Figure 3. Segmentation and development of sand spits along lakeshore of Lagoa de Mangueira in Brazil [7].

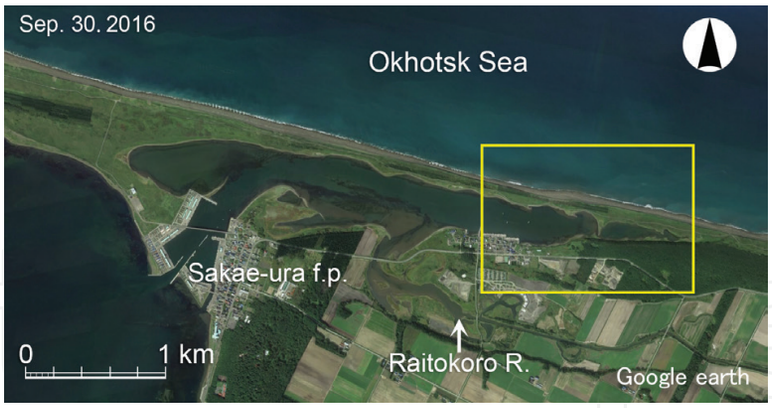

Figure 4. Study area in eastern Lake Saroma [10].

this fishing port, the width of the water body gradually decreases, and sand spits A-E develop together with pairs of sand spits A′ and E′. Of these sand spits, sand spits A and A′ are the largest and divide the water body into two. In the vicinity of sand spit A′, wind waves cannot be generated in the presence of the westerly wind, resulting in no development of sand spits. However, east of sand spit A′, wind waves can develop, and the size of the sand spits increases eastward in the order of sand spits B, C, and D.

2.3. Lakeshore in Lake Kitaura

Lake Kitaura located in Ibaraki Prefecture is a shallow lake with an area of 35.2 km^2 and 25 km length in the north-south direction, as shown in **Figure 6**. The formation of cuspate forelands in this lake was discussed in [5], and here we refer this results. This lake is located in the lowland surrounded by Kashima and Namegata tablelands with elevations of 40 and 30 m on the east and west sides, respectively. Thus, wind waves can be generated without a significant sheltering effect by hills or mountains. Because the direction of the principal axis of Lake

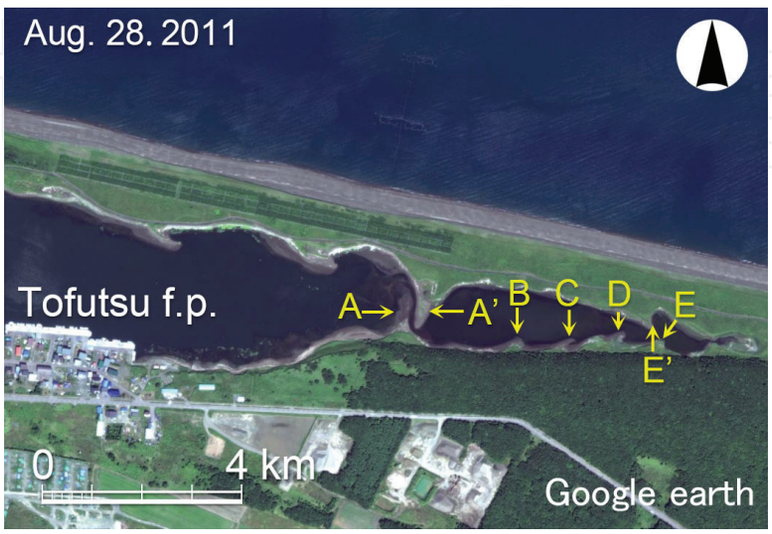

Figure 5. Enlarged satellite image of rectangular area in **Figure 4**, and sand spits A-E and E′ [10].

http://dx.doi.org/10.5772/intechopen.72550

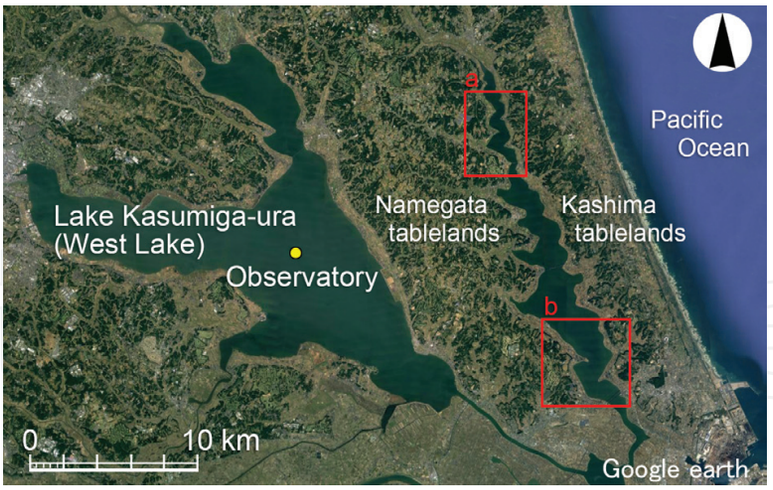

Figure 6. Cuspate forelands developed along lakeshore of Lake Kitaura in Japan [5].

Kitaura is N18°W, the predominant wind of NNE blows at an angle of 40.5° clockwise relative to the direction of the principal axis. Because of this oblique wind direction, wind waves are incident at a large incidence angle to the shoreline, resulting in the formation of the protruding shoreline on the west shore. In particular, an enlarged satellite image of two subareas, **a** and **b**, in **Figure 6** is shown in **Figure 7**. In subarea **a**, cuspate forelands and the ridges develop out of phase, and this condition is very similar to that in the lagoon facing the Chukchi Sea, as shown in **Figure 2**. Similarly, the cuspate forelands on both shores extend out of phase in subarea **b**. This shows a typical example of segmentation and the development of sand spits in a triangular lake.

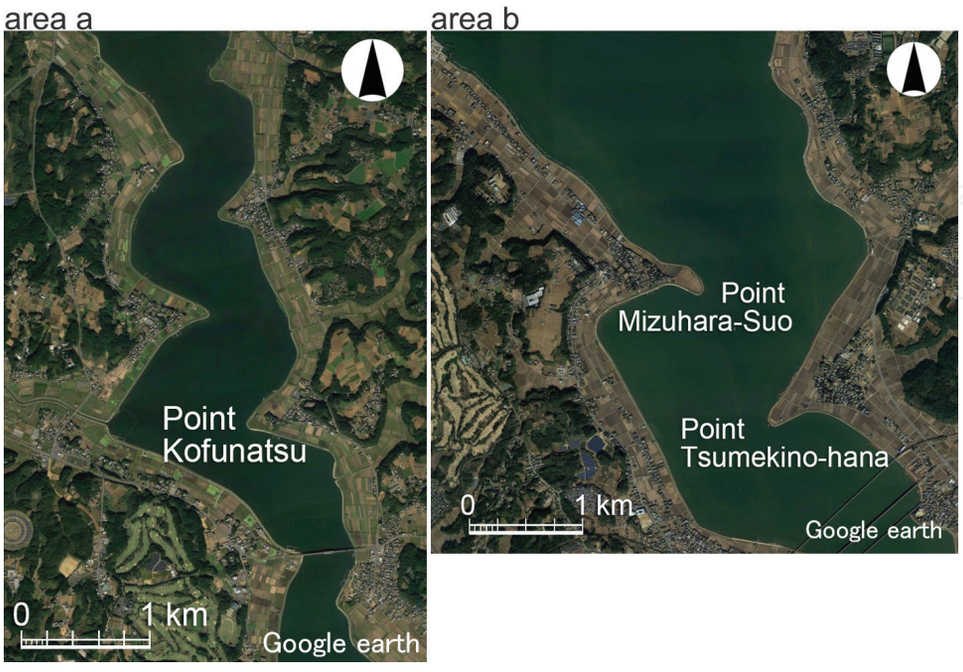

Figure 7. Enlarged satellite images of areas a and b in Lake Kitaura [5].

Figure 8. Satellite image of Lake Balkhash in Kazakhstan.

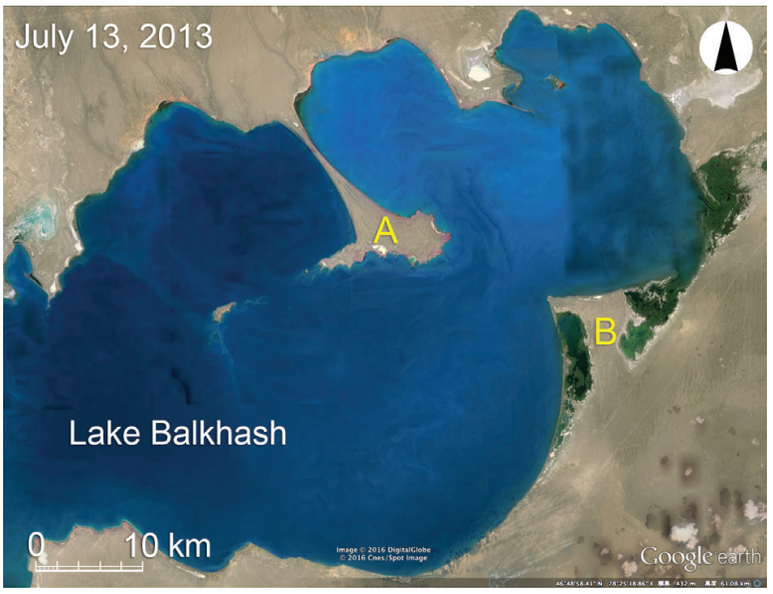

Figure 9. Enlarged satellite image of Lake Balkhash.

2.4. Lake Balkhash

Lake Balkhash has 450 and 200 km lengths in the E-W and S-N directions, respectively (**Figure 8**). **Figure 9** shows an enlarged satellite image of the rectangular area in **Figure 8**. Island A is located at a location of 46°34′53.99″N and 78°50′17.47″E at the central part of the lake near the east end, and a cuspate foreland of 14 km length extends between island A and the lakeshore. On the shore opposite to island A, a triangular cuspate foreland B is formed with a barrier island. The sand bar extending northwestward from Island A is symmetric with respect to the centerline of the cuspate foreland, and the length of the sand bar is longer than the width of the island. From this, it is inferred that the cuspate foreland extended from the land to Island A by the sand supply from Island A and the land, and connected to Island A.

http://dx.doi.org/10.5772/intechopen.72550

3. Model for predicting lakeshore changes

For the calculation of the segmentation of a rectangular water body, the BG model employed for the calculation of oriented lakes [8] was used. Given a local fetch distance F at a given point (g is the acceleration due to gravity and U is the wind velocity), the significant wave height $H_{1/3}$ was calculated using Wilson's formula [11, 12].

$$H_{1/3} = f(F, U) = 0.30\left\{1 - \left[1 + 0.004\left(gF/U^2\right)^{1/2}\right]^{-2}\right\}\left(U^2/g\right) \tag{1}$$

In this calculation, a coordinate system (x_w, y_w) was set corresponding to the wave direction instead of a fixed coordinate system (x, y) for the calculation of beach changes with the rectangular calculation domain, ABCD, as shown in **Figure 10**, and the wave height was calculated in the rectangular domain A'B'C'D' including the domain ABCD. Neglecting the wave refraction effect, waves were assumed to propagate in the same direction as the wind. The fetch distance F was added from upwind to downwind along the x_w-axis using Eq. (2) when the x_w-axis was divided by mesh intervals Δx_w [13]. Here, the index i in Eq. (2a) is the mesh number along the x_w-axis.

$$\mathrm{F}^{(i+1)} = F^{(i)} + \mathrm{r}\Delta x_w \tag{2a}$$

$$\mathrm{r} = \begin{cases} 1 & (Z \le 0) \\ 0 & (Z > 0) \end{cases} \tag{2b}$$

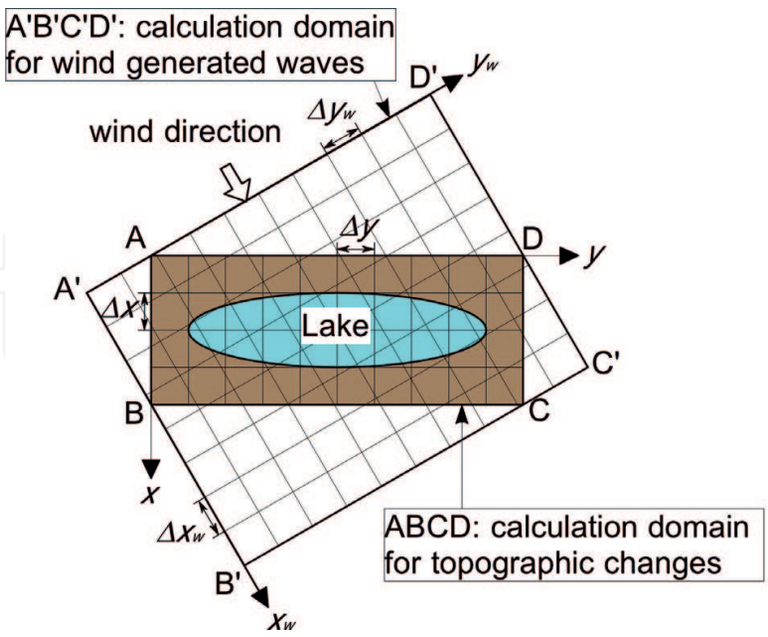

Figure 10. Selection of coordinate system (x, y) adopted for calculation of beach changes with rectangular calculation domain ABCD and another coordinate system (x_w, y_w) [13].

When a grid point was located on land and the downslope condition of $dZ/dx_w \leq 0$ was satisfied, the local fetch was reset as $F = 0$ (Eq. (3)).

$$F^{(i)} = 0 \quad \left(\text{if } Z \geq 0 \text{ and } dZ/dx_w \leq 0\right) \tag{3}$$

When the grid point was located in the lake, F was recalculated. By this procedure, the wave height becomes 0 on the lee of the cuspate forelands, and the wave-sheltering effect alone can be evaluated.

For the sand transport equation, Eq. (4), which is expressed using the wave energy at the breaking point, was used [6].

$$\vec{q} = C_0 \frac{K_s P}{\tan\beta_c} \left\{ \tan\beta_c \vec{e}_w - |\cos\alpha| \overrightarrow{\nabla Z} \right\} \quad \left(-h_c \leq Z \leq h_R\right) \tag{4}$$

$$P = \varepsilon(Z) \left(EC_g\right)_b \tan\beta_w \tag{5}$$

$$\tan\beta_w = dZ/dx_w \quad \left(\tan\beta_w \geq 0\right) \tag{6}$$

Here, $\vec{q} = (q_x, q_y)$ is the net sand transport flux, $Z(x, y, t)$ is the seabed elevation with reference to the still water level ($Z = 0$), $\overrightarrow{\nabla Z} = (\partial Z/\partial x,\ \partial Z/\partial y)$ is the seabed slope vector, $\vec{e}_w$ the unit vector of the wave direction, α is the angle between the wave direction and the direction normal to the contour line, and $|cos\alpha| = |\vec{e}_w \cdot \overrightarrow{\nabla Z}|/|\overrightarrow{\nabla Z}|$. $\tan\beta_c$ is the equilibrium slope of sand, and K_s is the longshore and cross-shore sand transport coefficient. The P value in Eq. (5) is the wave dissipation ratio per unit area of the seabed and time between $Z = -h_c$ and h_R, where sand movement occurs [6], and $(EC_g)_b$ is the wave energy flux at the breaking point. x_w is the coordinate in the direction of wave propagation, and $\tan\beta_w$ is set to 0 when $\tan\beta_w < 0$ is satisfied. $\tan\beta_w$ is the seabed slope measured in the direction of wave propagation. In the calculation, the local beach slope measured along the wave ray was used for the beach slope in Eq. (5), as shown in Eq. (6). h_c is the depth of closure, and h_R is the berm height. C_0 is the coefficient for transforming the immersed weight expression to the volumetric expression ($C_0 = 1/\{(\rho_s - \rho)g(1-p)\}$; ρ is the seawater density, ρ_s is the specific gravity of sand, p is the sand porosity, g is the acceleration due to gravity), $\varepsilon(Z)$ in Eq. (5) is the depth distribution of sand transport and is defined so as to satisfy Eq. (7); in this study, a uniform distribution was employed (Eq. (8)).

$$\int_{-h_c}^{h_R} \varepsilon(Z) dZ = 1 \tag{7}$$

$$\varepsilon(Z) = 1/\left(h_c + h_R\right) \quad \left(-h_c \leq Z \leq h_R\right) \tag{8}$$

If $H_{1/3}$ is approximately equal to the breaker height H_b and γ is the ratio of the breaker height to water depth, the wave energy flux at the breaking point $(EC_g)_b$ in Eq. (5) can be written as Eq. (9a).

$$\left(E\,C_g\right)_b = C_1 \left(H_b\right)^{\frac{5}{2}} \approx C_1 \left(H_{1/3}\right)^{\frac{5}{2}} \tag{9a}$$

$$C_1 = \frac{\rho g}{k_1}\sqrt{g/\gamma} \quad \left(k_1 = (4.004)^2, \gamma = 0.8\right) \tag{9b}$$

When F and $H_{1/3}$ are calculated using the coordinate system (x_w, y_w) according to the wave direction, the wave power P (Eq. (5)) can be calculated and assigned to each grid point on the coordinate system (x_w, y_w). The wave power P at each grid point in the calculation of beach changes was interpolated from this distribution of P. The mesh intervals (Δx_w, Δy_w) in the coordinate system (x_w, y_w) were taken to be the same as (Δx, Δy). Finally, the sand transport and continuity equations were solved on the x-y plane by the explicit finite-difference method using a staggered mesh scheme. In this study, the wind direction at each step in the calculation of beach changes was selected to be a value determined by random numbers so as to satisfy the probability distribution function of the occurrence of a certain wind direction, although the wind velocity was assumed to be constant.

In estimating the intensity of sand transport near the berm top and at the depth of closure, the intensity of sand transport was linearly reduced to 0 near the berm height or the depth of closure to prevent sand from being deposited in the zone higher than the berm height and the beach from being eroded in the zone deeper than the depth of closure [14].

4. Calculation conditions

Lakeshore changes in a rectangular water body with an aspect ratio of 5 owing to wind waves were first predicted when wind blew from all directions between 0 and 360° with the same probability of occurrence and intensity (Case 1) or blew at an angle of 45° relative to the principal axis of the rectangular water body with an elliptic probability of occurrence and intensity (Case 2), as shown in **Figure 11** [13]. Then, lakeshore changes in triangle- and crescent-shaped shallow water bodies with a flatbed were predicted in Cases 3 and 4, respectively. In all cases, the water depth of the flatbed, the berm height, and the initial beach slope were set to 3 m, 1 m, and 1/20, respectively. **Figure 12** shows the initial topography in each case. Random perturbations with

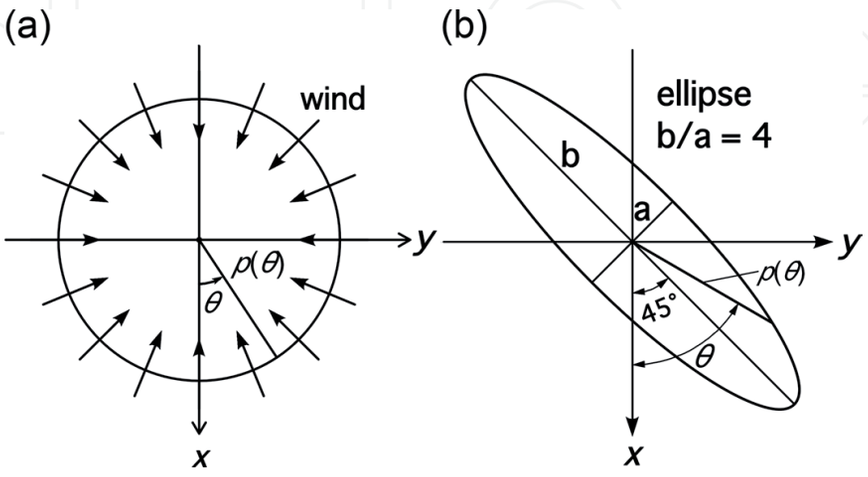

Figure 11. Probability distribution of occurrence of wind direction: (a) circular and (b) elliptic [13].

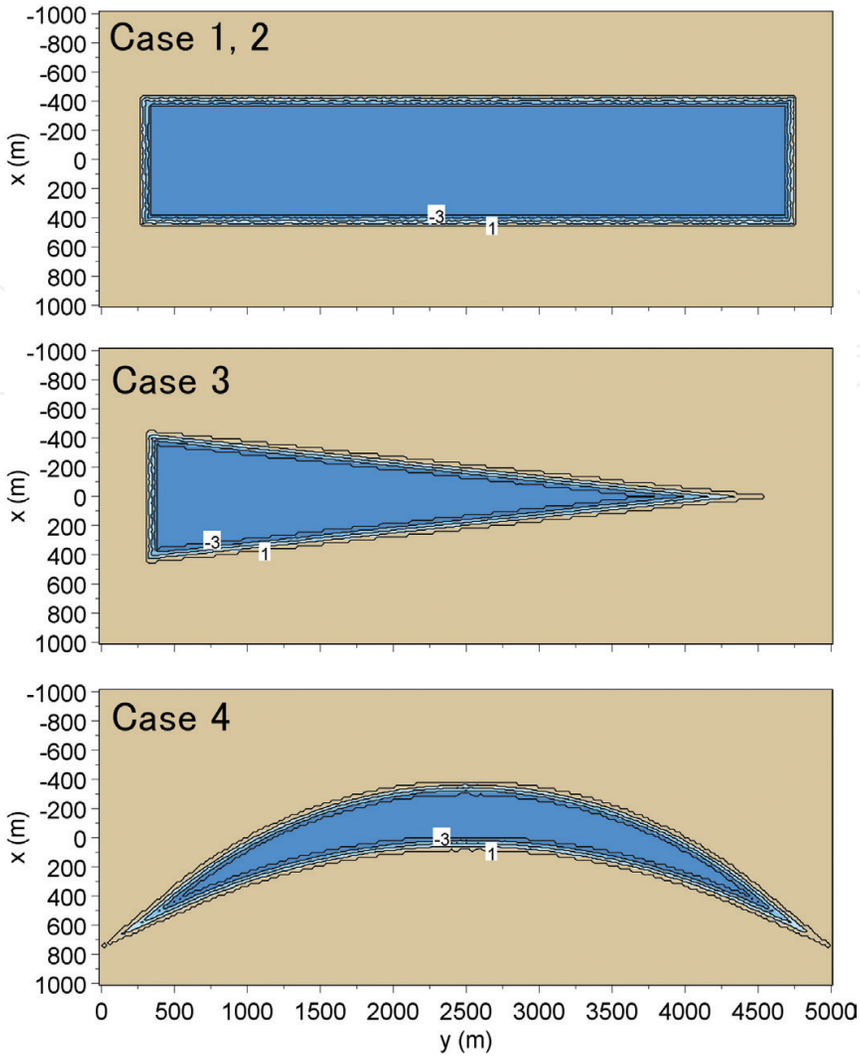

Figure 12. Initial topographies in Cases 1–4.

the amplitude $\triangle Z = 0.1$ m were added to the slope between $Z = 1$ and -3 m in the initial bathymetry. The wind velocity was 20 m/s. The calculation domain was discretized by $\triangle x = \triangle y = 20$ m with $\triangle t = 10$ h. The depth distribution of sand transport was assumed to be a uniform distribution throughout the depth, and the equilibrium slope was 1/20. **Table 1** shows the calculation conditions for Cases 1–4. The wind velocity of 20 m/s is the value at which a significant wave height of approximately 1 m, the same as the berm height, could be generated, given the fetch distance of 4.6 km, being the distance along the diagonal of the initial rectangular water body in Cases 1 and 2. In Cases 3 and 4, the wind velocity was also assumed to be 20 m/s, and wind was assumed to blow from all directions with the same probability and intensity.

In predicting lakeshore changes when a rocky or sandy island is located in a closed water body, four calculations were carried out, as shown in **Figure 13**. In each case, a circular lake with a radius of 1000 m and a solid bottom of a constant depth of 3 m was set for the calculation domain. In this circular lake, a rocky or sandy island with a radius of 200 m was set at locations deviating from the center of the lake. The foreshore slope of the lakeshore was assumed to be 1/20. In the present study, the incident angle of waves to the mean shoreline exceeds 45° at

Wind velocity	20 m/s
Berm height, h_R	1 m
Depth of closure, h_c	3 m
Equilibrium slope, $\tan\beta_c$	1/20
Coefficient of sand transport	$K_s = 0.2$
Calculation cases	Case 1: rectangular water body, circular probability distribution
	Case 2: rectangular water body, elliptic probability distribution
	Case 3: segmentation of a triangular water body
	Case 4: segmentation of a crescent-shaped water body
	Cases 5–8: topographic changes around an island located in a circular lake
Mesh size	$\Delta x = \Delta y = 20$ m
Time intervals	$\Delta t = 10$ h
Duration of calculation	10^6 h (10^5 steps) in Cases 1–4,
	5×10^5 h (5×10^4 steps) in Cases 5–8
Boundary conditions	Shoreward and landward ends, $q_x = 0$
	Right and left boundaries, $q_y = 0$

Table 1. Calculation conditions.

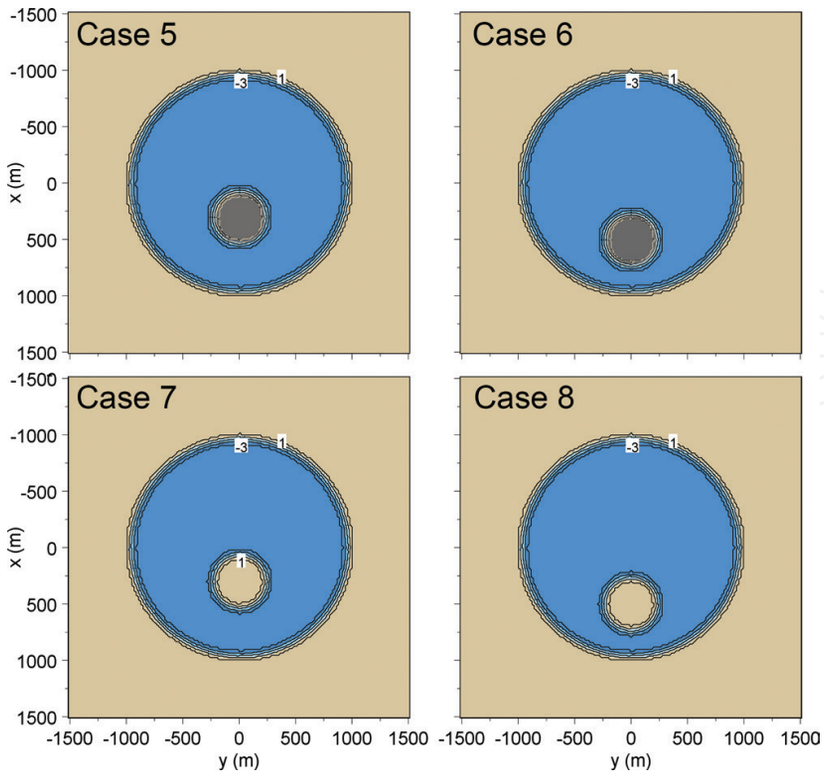

Figure 13. Arrangement of island in Cases 5–8.

certain locations of the lakeshore, resulting in shoreline instability. Therefore, a small perturbation with the amplitude $\Delta Z = 0.1$ m was added in the depth zone between $Z = -3$ and 1 m. In Cases 5 and 6, a rocky island was placed with its center deviating from the center of lake, and the wave-sheltering effect by the island was enhanced in Case 6, in which the island was set at a location closer to the lakeshore. In Cases 7 and 8, the arrangement of the island is the same as those in Cases 5 and 6, respectively, but the island is composed of sand. The other conditions are the same as those in Cases 1–4. **Table 1** shows the calculation conditions for Cases 5–8.

5. Results

5.1. Segmentation of water body given circular distribution of probability (Case 1)

Figure 14 shows the calculation results for the segmentation of a slender, rectangular water body with a longshore length of 4.5 km, and a width of 0.9 km (aspect ratio = 5), assuming that the probability of occurrence of wind direction was given by a circular distribution [13]. When wind waves were incident to the lakeshore, several cuspate forelands with irregular shapes developed along the shoreline in the beginning. After 2×10^4 steps, the cuspate forelands merged with each other, resulting in a reduction in their number, and sand bars with a hound's-tooth shape were formed. This development of cuspate forelands well explains the formation of the lakeshore, as shown in **Figure 2**. After 4×10^4 steps, sand bars extended to the opposite shores, and the water body was about to separate into two lakes, and then the water body had separated into two completely independent lakes. Finally, two completely rounded lakes were formed.

The distributions of the wave height and longshore sand transport alter in response to the wind direction at each time. The formation of cuspate forelands and rounded lakes over time, however, strongly depends on the mean $(H_{1/3})^{5/2}$ flux averaged over a significantly long time [13]. **Figure 15** shows the mean $(H_{1/3})^{5/2}$ flux averaged over 10^3 steps at six stages between 1×10^3 and 1×10^5 steps. The arrows in the figure show the direction of the flux, and the color corresponds to the intensity of the flux. After 10^3 steps, outward flux was generated radially from the central part of the lake with a symmetric distribution, and the time-averaged flux at the central part was 0 because of the cancelation of the sum of the vectors. After 2×10^4 steps, the mean $(H_{1/3})^{5/2}$ flux was equivalent on both sides of the central cuspate foreland, facilitating the development of the cuspate foreland. After 4×10^4 steps, the cuspate forelands had further developed, and the direction of the mean $(H_{1/3})^{5/2}$ flux approached the direction normal to the shoreline. Finally, after 10^5 steps, its direction became normal to the shoreline of the rounded lake.

The mean sand transport flux after 4×10^4 and 5×10^4 steps in Case 1 can be drawn, as shown in **Figure 16** [13]. Intensive sand transport flux occurred along the shoreline of a cuspate foreland at the central part of the water body, enhancing further development of a cuspate foreland. Also, intensive sand transport took place near the right corner of the slender water body because of a large aspect ratio of the water body, which induced the formation of a circular lake.

5.2. Segmentation of water body given elliptic distribution of probability (Case 2)

In Case 2, wind blew from the direction of 45° with respect to the principal axis of the slender lake, that is, the probability of occurrence of the wind direction is given by an elliptic distribution [13].

http://dx.doi.org/10.5772/intechopen.72550

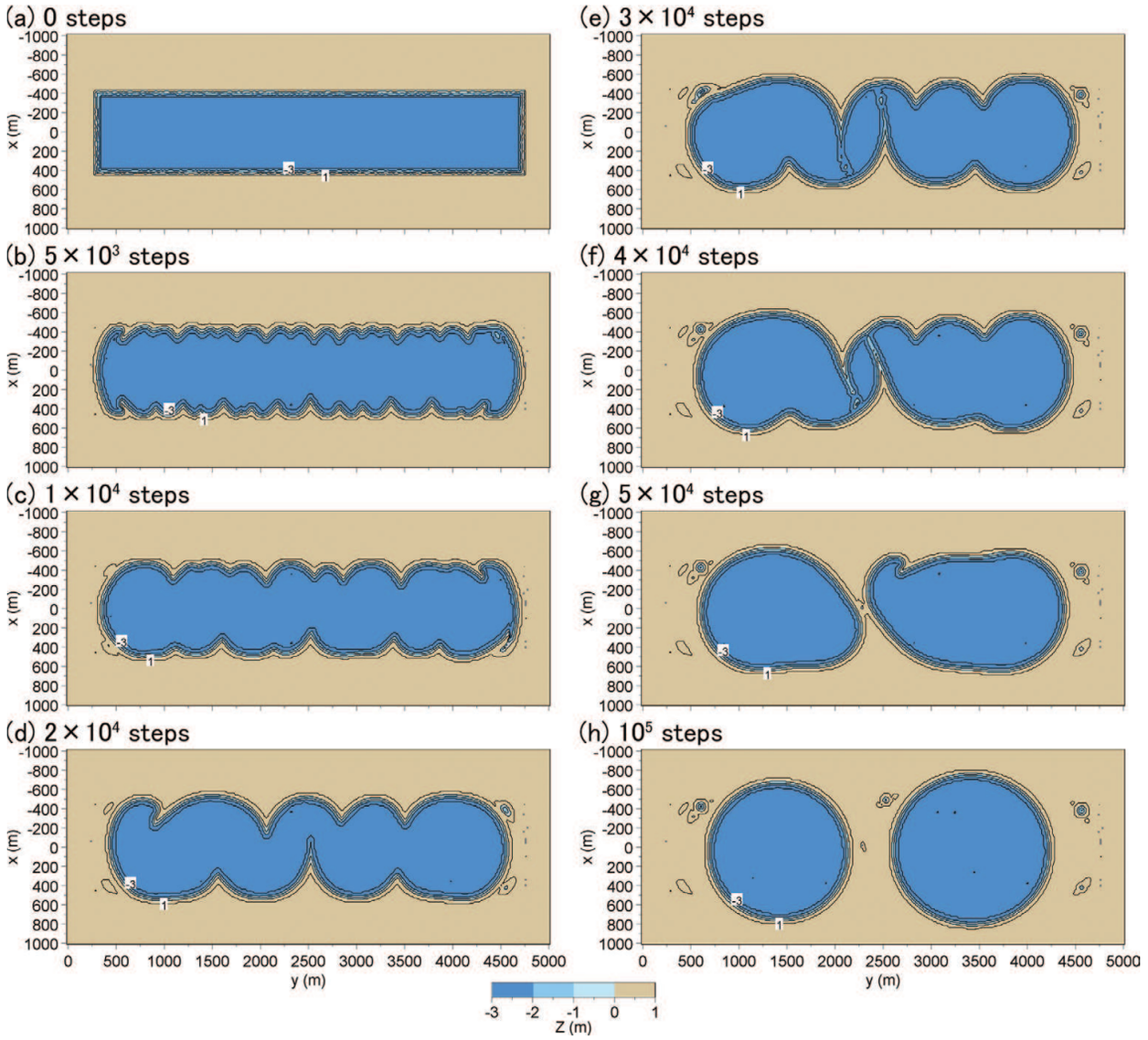

Figure 14. Topographic changes in Case 1 under uniform distribution of occurrence of wind direction and intensity [13].

Uda et al. [8] predicted the formation of oriented lakes [15] using the BG model and showed that oriented lakes can develop when the probability of occurrence of the wind direction is given by an elliptic distribution. Here, the segmentation of a rectangular water body was predicted, assuming that the probability of occurrence was given by an elliptic distribution.

Figure 17 shows the predicted results of the lake averaged over 10^3 steps in Case 2 [13]. Cuspate forelands with an asymmetric form had developed on both shores and inclined rightward (leftward) on lower (upper) shorelines in the beginning. Then, the cuspate forelands had merged to increase their size and moved rightward (leftward) on lower (upper) shorelines. These results are in good agreement with those obtained by Uda et al. [5] concerning the development of sand spits and cuspate forelands owing to the shoreline instability. Because the principal axis of the wind direction is at an angle of 45° relative to the shoreline, and the effect of wind blowing from the land to the lake can be neglected along lower shoreline, the oblique component of waves incident from the left had a higher probability than that of waves incident from the right. As a result, rightward sand transport predominantly

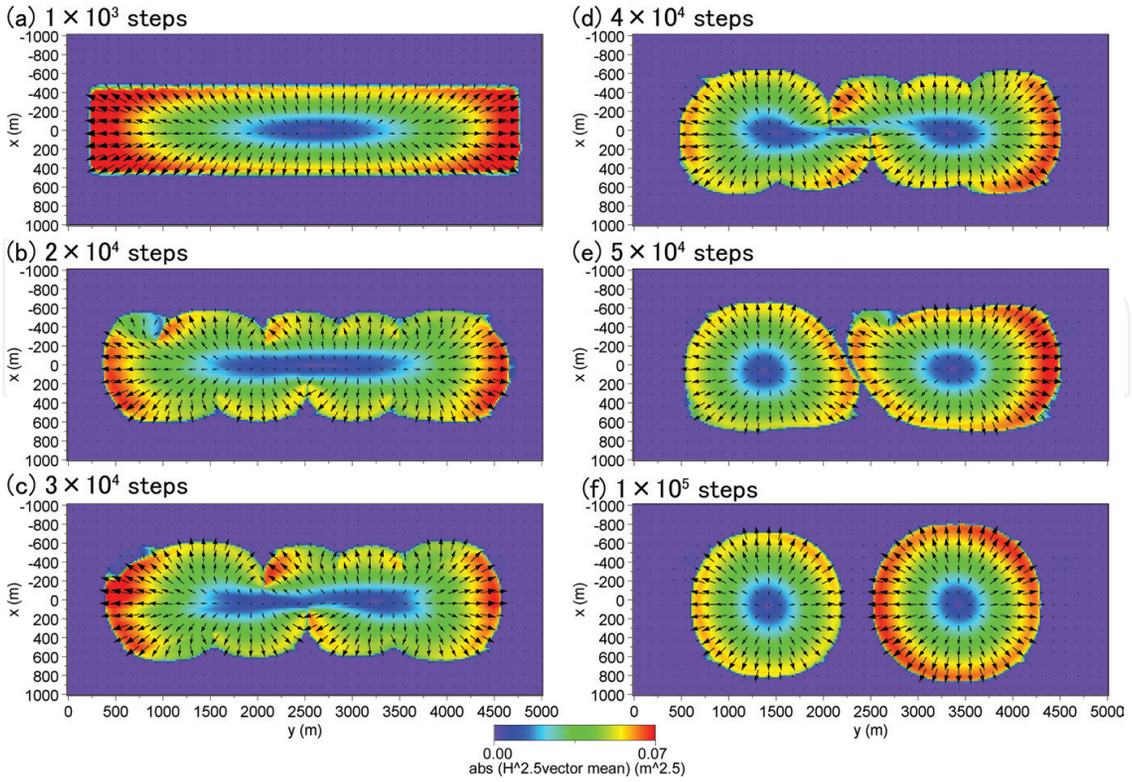

Figure 15. Distribution of mean $(H_{1/3})^{5/2}$ flux in Case 1 [13].

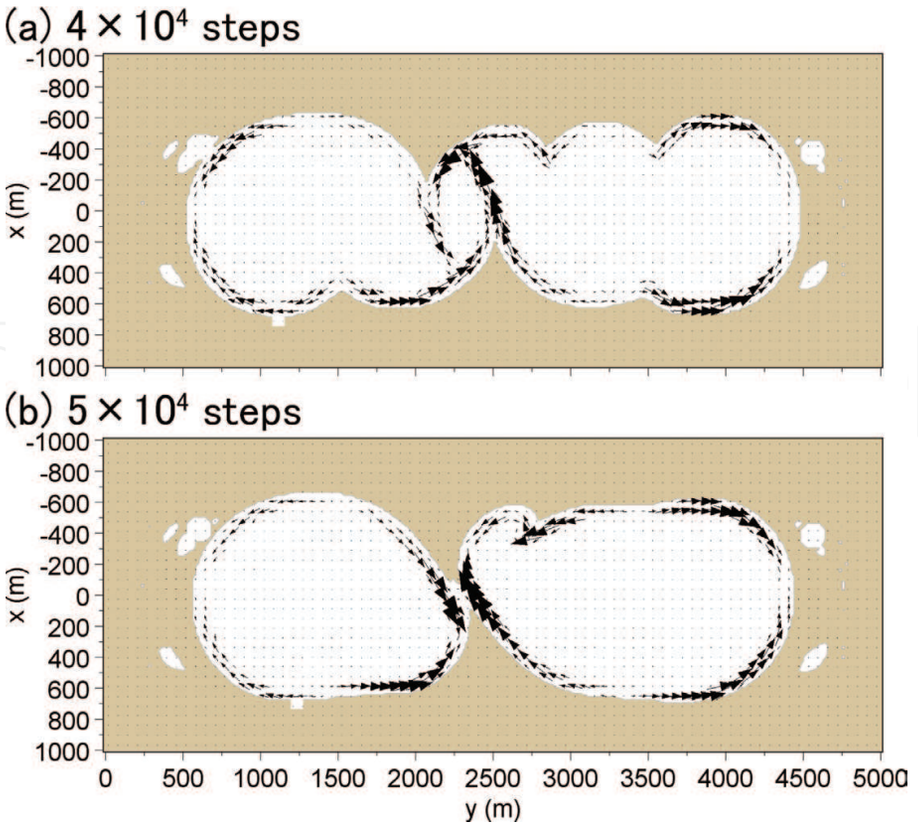

Figure 16. Mean sand transport flux in Case 1 [13].

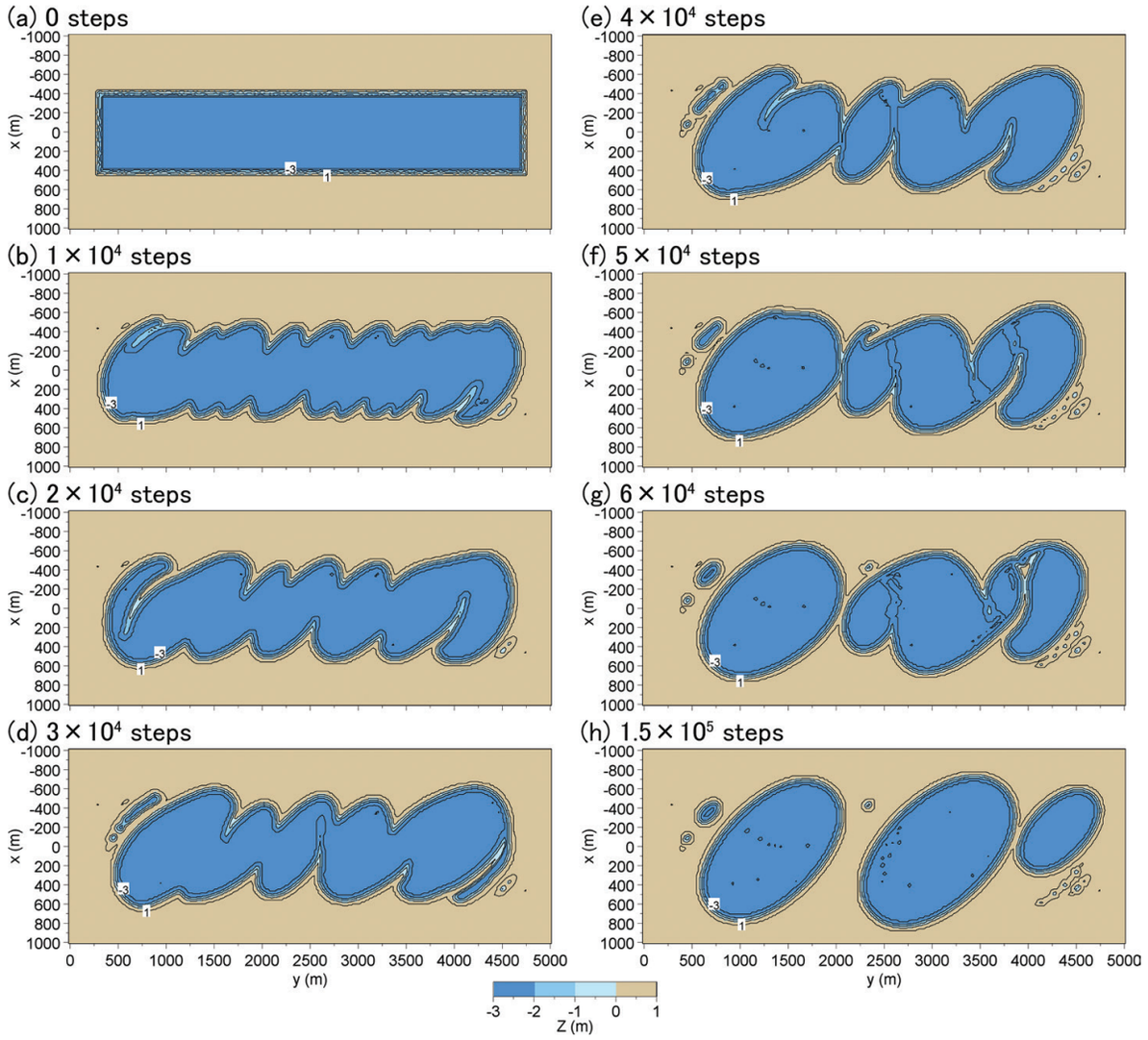

Figure 17. Topographic changes in Case 2 under elliptic distribution of occurrence of wind direction [13].

caused the formation of a cuspate foreland with an asymmetric shape along the *y*-axis, and rightward movement of the cuspate foreland took place. The formation of a cuspate foreland with an asymmetric shape corresponds to the formation of a lagoon, as shown in **Figure 2**. Furthermore, the cuspate foreland markedly developed at the right (left) end on the lower (upper) shoreline because of the long fetch distance and large wave intensity after 2×10^4 steps. With time, the cuspate forelands near the end of the lake were connected to the ends and formed a barrier island, whereas the cuspate foreland in the central part markedly extended to the opposite shore. After 5×10^4 steps, the water body on the left side was segmented to have an elliptic form. Finally, three segmented lakes with an elliptic shape were formed. The formation of the lakes with an elliptic shape with parallel principal axes explains the development process of the elliptic lakes observed in Chukchi Sea shown in **Figure 1**.

5.3. Segmentation of a triangular or crescent-shaped water body (Cases 3 and 4)

Figure 18 shows the results of the calculation of the segmentation of a triangular water body, assuming that the probability of occurrence of wind direction was given by a circular

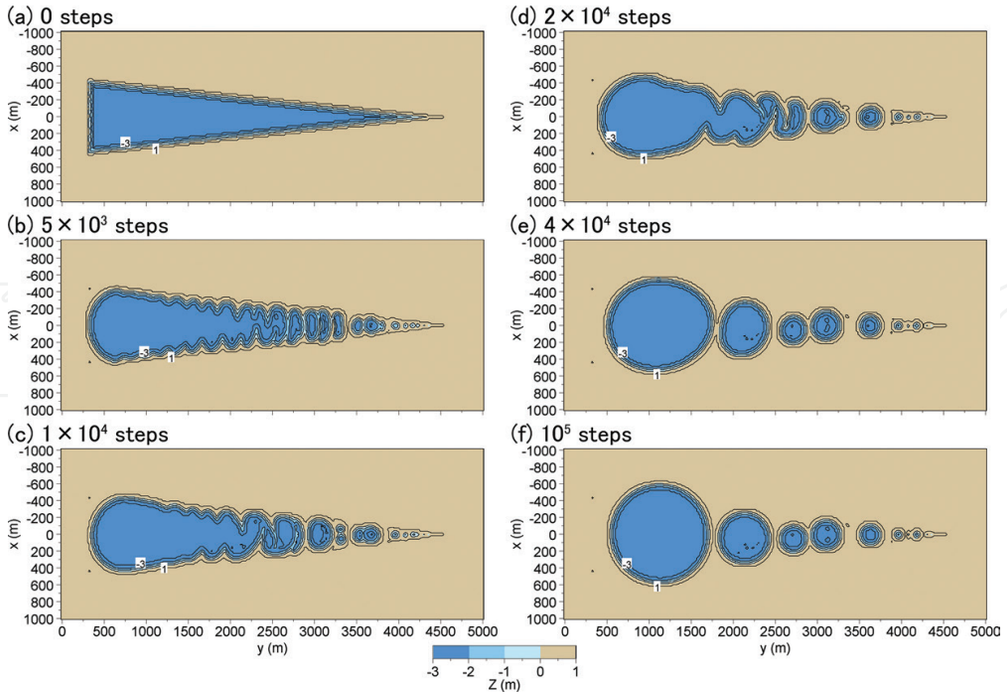

Figure 18. Segmentation of a triangular water body with time.

distribution [7]. Although the results are similar to those in [7], numerical simulation was carried out with changing the size of the lake because of the revision in Eq. (2b). Segmentation rapidly occurred in the vicinity of the right end of the triangular water body, and elliptic lakes were formed in the area between $y = 3.25$ and 3.75 km in the beginning. Near the left end, the segmentation stage was delayed, and cuspate forelands extended from both shores. After 1×10^4 steps,

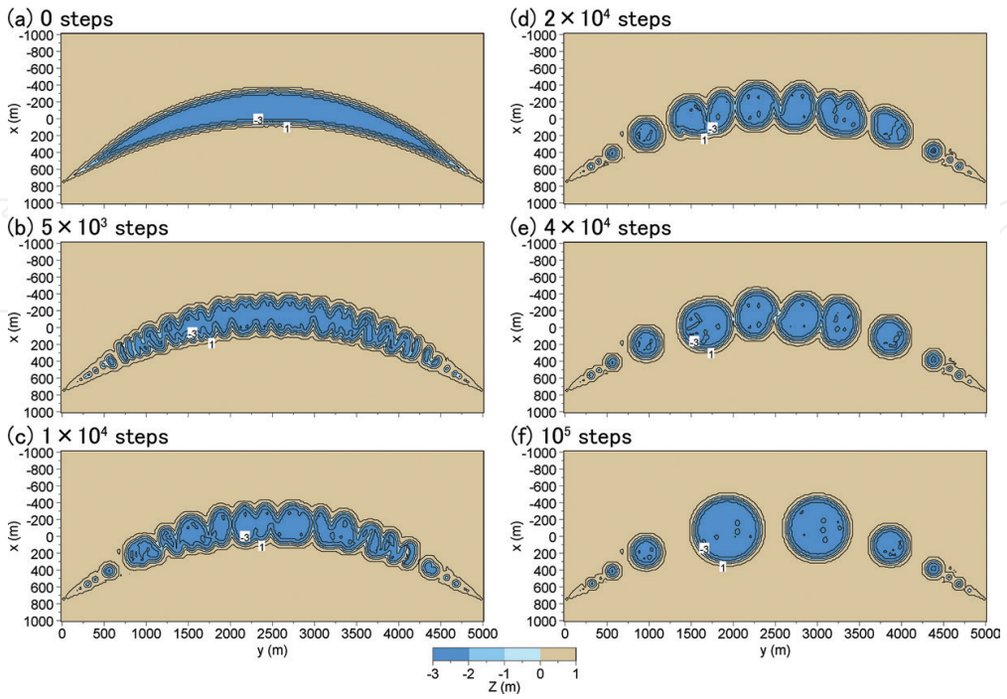

Figure 19. Segmentation of a crescent-shaped water body with time.

the elliptic lake that formed near y = 3.0 km became rounded and merged into a larger lake, resulting in a decrease in the aspect ratio. Until 4×10^4 steps, five circular lakes were formed. The shape of the water body after 1×10^4 steps well explains the development of the sand spits in Lake Saroma shown in **Figure 5**.

Similarly, **Figure 19** shows the results of the segmentation of a crescent-shaped water body with time. Rapid segmentation occurred in the vicinity of the both ends of the crescent water body in the beginning. In the area between y = 3.25 and 4.0 km, cuspate forelands that developed from both shores were alternately distributed on both shores, in contrast to the symmetric cuspate forelands in the central part. This explains the features observed in the water body facing the Chukchi Sea, as shown in **Figure 2**. After 1×10^4 steps, sand bars with a hound's-tooth shape were formed in the area between y = 3.75 and 4.25 km. The segmentation continued over time, and the lakes became rounded as a whole. After 10^5 steps, circular lakes with a radius corresponding to the initial lake width were formed and stabilized.

5.4. Lakeshore changes in circular lake with a rocky or sandy island

Figure 20 shows the lakeshore changes in Case 5 with a rocky island in a circular lake, assuming that the probability of occurrence of wind direction was given by a circular distribution. Under

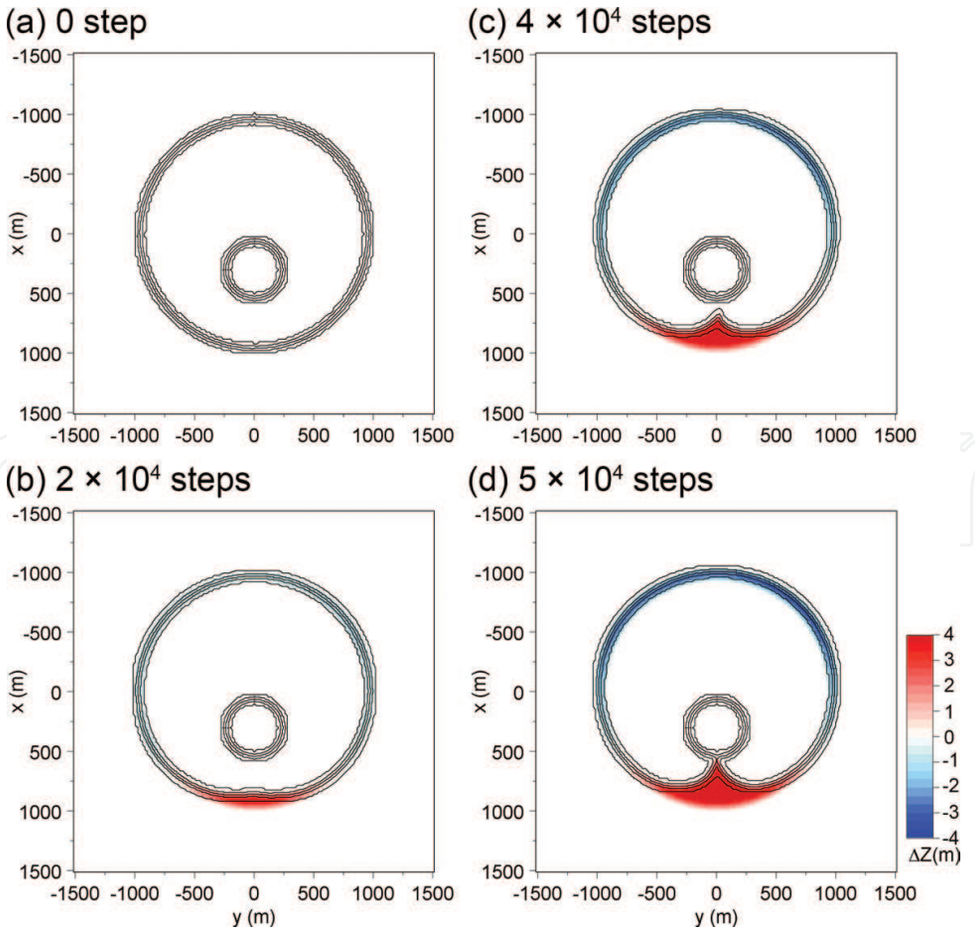

Figure 20. Lakeshore changes behind a rocky island in lake (Case 5).

the condition, a wave-shelter zone was primarily formed on the lee of the island against wind waves incident from x-axis. Sand was transported from the outside of the wave-shelter zone to the inside, and a symmetrical cuspate foreland started to form on the lee of the island. After 5×10^4 steps, the cuspate foreland connected to the island. Because sand was mainly transported from the opposite shore with a longer fetch distance to the lee of the island, the lakeshore on the opposite shore was eroded. Thus, when a rocky island is asymmetrically located at a location in a lake, the formation of a cuspate foreland and erosion on the opposite shore take place at the same time.

Figure 21 shows the same results in Case 6. In this case, the wave-sheltering effect due to the island was strengthened than that in Case 5 because of the proximity of the island to the lakeshore, the cuspate foreland rapidly developed together with the formation of a large cuspate foreland. After 5×10^4 steps, a headland with a circular head was formed. Because the distance between the island and lakeshore decreased, the wave-sheltering effect increased, resulting in the greater cuspate foreland behind the island and erosion on the opposite shore.

The lakeshore changes in Case 7 with a sandy island in a circular lake are shown in **Figure 22**. When waves were incident to the sandy island, the island deformed by the action of waves incident from x-axis, which has the longest fetch distance, and slender sand bars extended

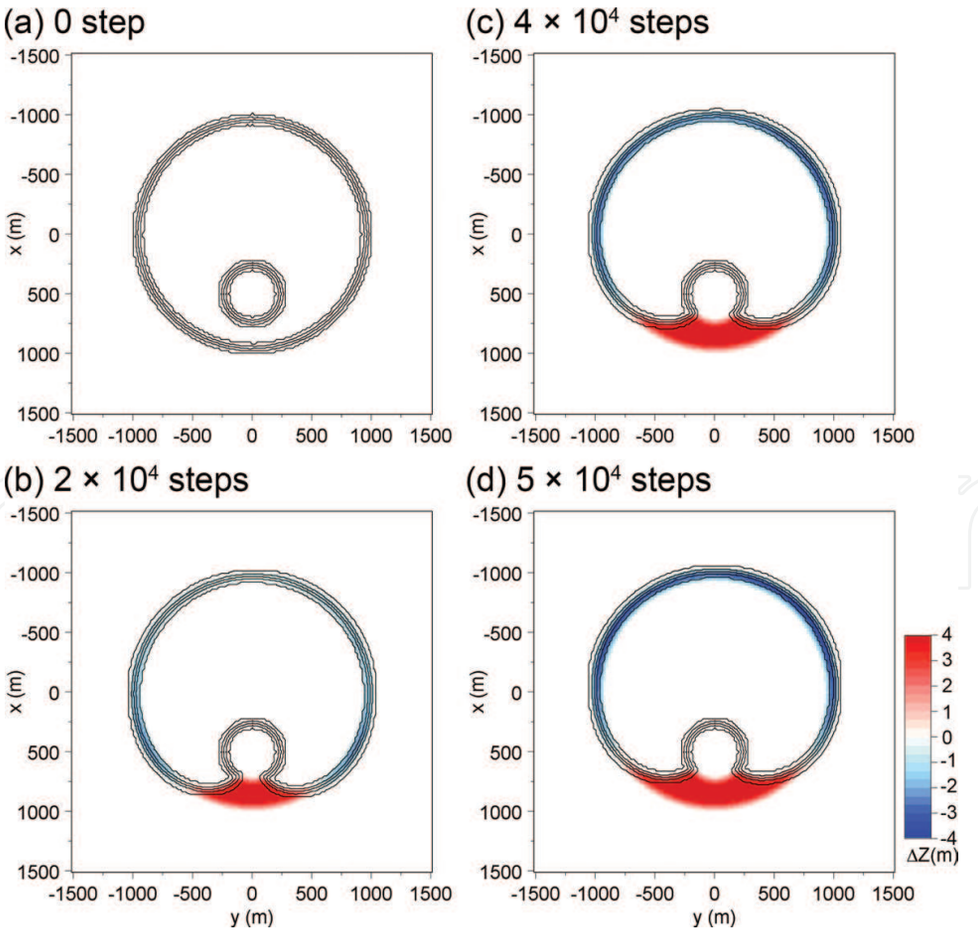

Figure 21. Lakeshore changes behind a rocky island in lake (Case 6).

http://dx.doi.org/10.5772/intechopen.72550

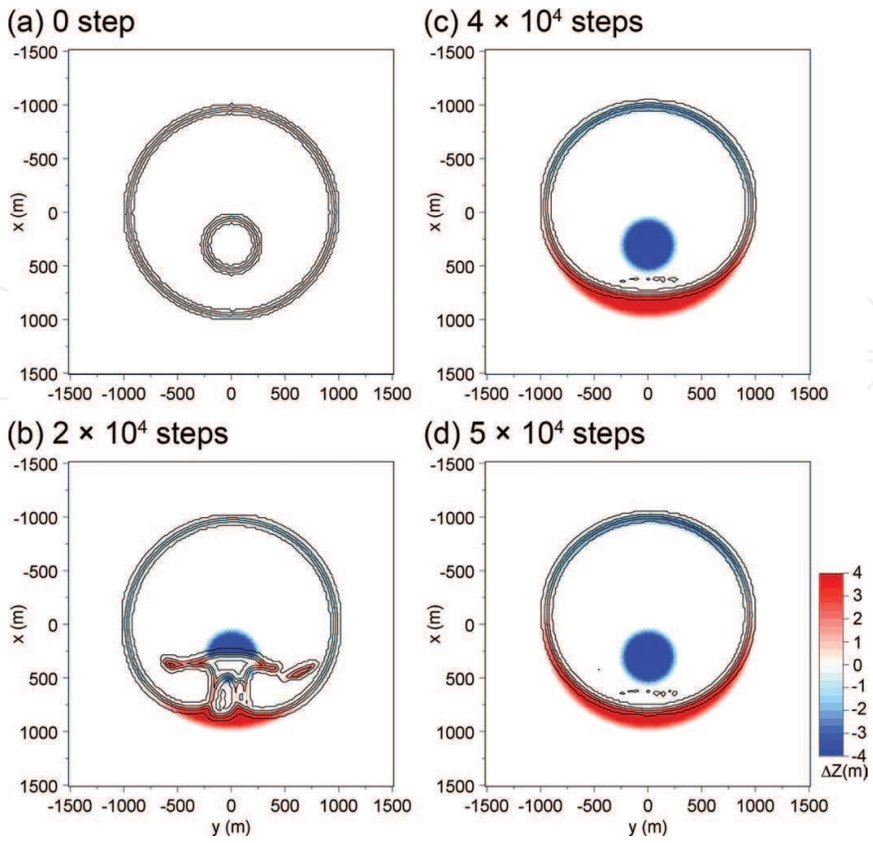

Figure 22. Lakeshore changes around a sandy island in lake (Case 7).

toward the *y*-axis. In the wave-shelter zone of this sand bars, double tombolo extended at first, which connected to the slender sand bars. With time, all sand comprised of the island were transported to the lakeshore and merged with the lakeshore. After 5×10^4 steps, a large amount of sand was deposited on the lee of the island, whereas the opposite shore was eroded.

Figure 23 shows the same results in Case 8. The initial circular island significantly deformed owing to the action of wind waves incident from the direction of *x*-axis, and sand bars extending to the direction of the *y*-axis were formed. Because of the short distance between the island and lakeshore, double tombolo quickly extended on the lee of the sandy island, while leaving a lagoon in the central part. With time, a barrier island was formed with a lagoon inside double tombolo, and the smaller lake behind the barrier island was rounded by wind waves in the closed water body. A large amount of sand was deposited behind the island.

The mean sand transport fluxes averaged over 1000 steps between $1.9 \times 10^4 + 1$ and 2×10^4 steps in Cases 5 and 7 with the same arrangement of an island are shown in **Figure 24**. In Case 5 with a rocky island, the intensive sand transport flux occurred on both sides of the island with decreasing the intensity behind the island, whereas in Case 7, strong sand transport flux toward the tips of the sand bar occurred along the shoreline of sand bars. When setting point O at the center of the circular lake, and points **a** and **b** at both ends of the straight line through point O, as shown in **Figure 24**, the direction of sand transport flux is downward at points **a** and **b**. Out of waves incident to point **a**, waves incident from the upper half of the

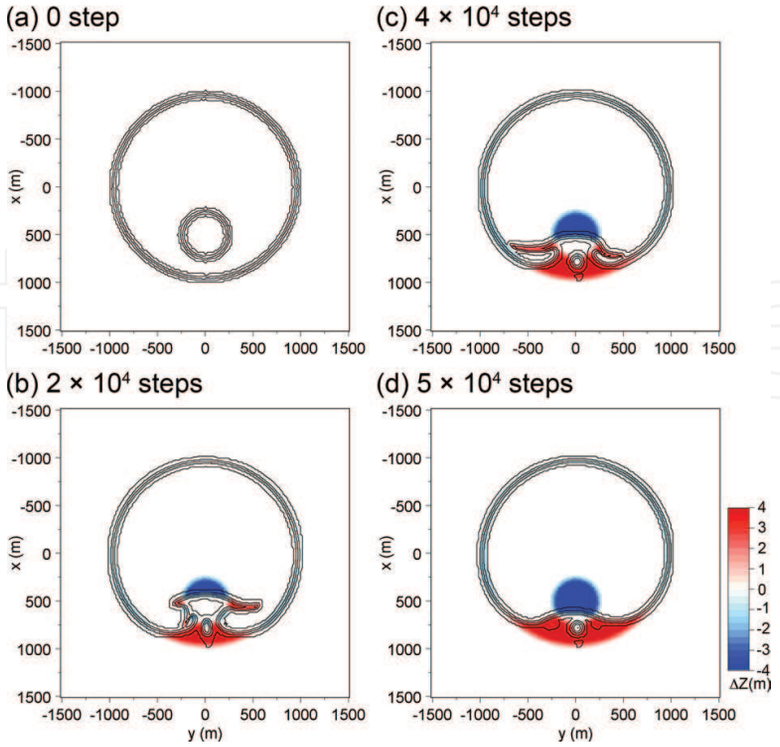

Figure 23. Lakeshore changes around a sandy island in lake (Case 8).

lake causes downward longshore sand transport, and vice versa, when waves are incident from the lower half. Without an island, net sand transport at point A is 0 because of the symmetricity of the closed water body. With an island, however, the area of the water body in the lower half decreases than that in the upper half, resulting in weaker wave action. As a result, the direction of the net sand transport fluxes at points **a** and **b** became downward, enhancing sand transport from the upper half to the lower half, resulting in erosion in the upper half.

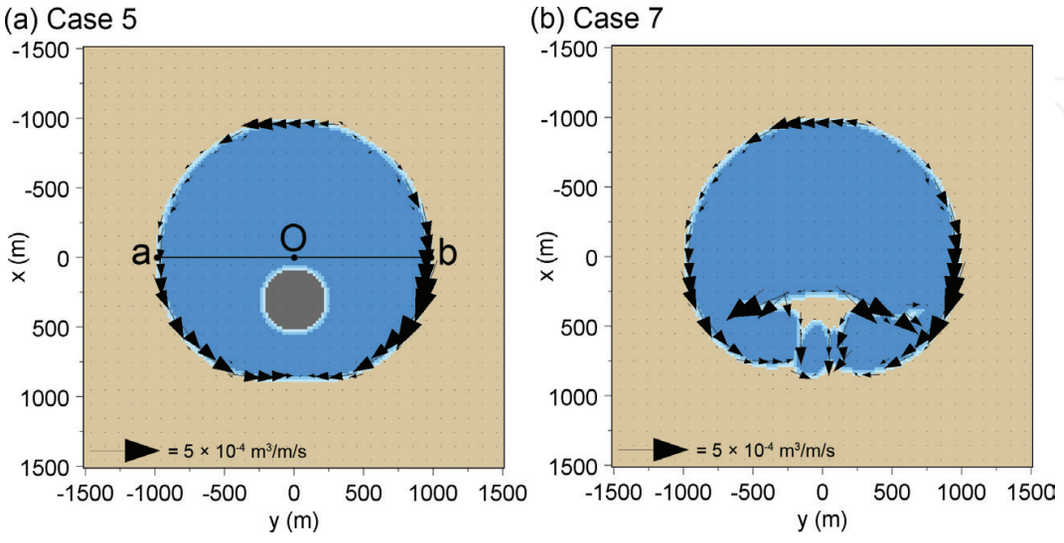

Figure 24. Mean sand transport flux averaged over 1000 steps in Cases 5 and 7.

In the case of Lake Balkhash, part of sand comprised of the island was considered to be transported northwestward, forming a long slender sand bar. Such topographic changes can be explained by the mergence of a slender sand bar extended from the island and the sand bar extended in the opposite direction, as shown in the results after 5×10^4 steps in Case 5 and after 2×10^4 steps in Case 7.

6. Conclusions

Specific geomorphological features associated with shoreline instability under a high-wave-angle condition on the lakeshore, such as the development of sand spits, in several elongated water bodies were investigated, and the segmentation of a water body was numerically predicted using the BG model. It was concluded that a rectangular water body segmented into circular (elliptic) lakes when the probability of occurrence of the wind direction was given by a circular (elliptic) distribution. In each case, the wave-sheltering effect of the cuspate forelands played a primary role. Also, the mergence and segmentation of triangular and crescent-shaped slender water bodies were predicted using the BG model. It was further used for predicting the lakeshore changes when a rocky or sandy island exists in a circular lake. The deformation of a sandy island and mergence of the sandy island to the lakeshore were predicted well.

Author details

Takaaki Uda[1], Masumi Serizawa[2]* and Shiho Miyahara[2]

*Address all correspondence to: coastseri@nifty.com

1 Head, Shore Protection Research, Public Works Research Center, Taito, Tokyo, Japan

2 Coastal Engineering Laboratory Co., Ltd., Shinjuku, Tokyo, Japan

References

[1] Ashton A, Murray AB, Arnault O. Formation of coastline features by large–scale instabilities induced by high-angle waves. Nature. 2001;**414**:296-300

[2] Ashton A, Murray AB High-angle wave instability and emergent shoreline shapes: 1. Modeling of sand waves, flying spits, and capes. Journal of Geophysics Research. 2006;**111**:F04011. DOI: 10.1029/2005JF000422

[3] Zenkovich VP. Processes of Coastal Development. New York: Interscience Publishers; 1967. p. 751

[4] Ashton A, Murray AB, Littlewood R, Lewis DA, Hong P. Fetch limited self-organization of elongate water bodies. Geology. 2009;**37**:187-190

[5] Uda T, Serizawa M, Miyahara S. Numerical simulation of three-dimensional segmentation of elongated water body using BG model. Proc. 33rd ICCE, sediment. 65, 2012. pp. 1-11

[6] Serizawa M, Uda T, San-nami T, Furuike K. Three-dimensional model for predicting beach changes based on Bagnold's concept. Proc. 30th ICCE, 2006; pp. 3155-3167

[7] Uda T, Serizawa M, Miyahara S, San-nami T. Prediction of segmentation and mergence of shallow water bodies by wind waves using BG model. Proc. Coastal Dynamics. 2013; Paper No. 166, pp. 1729-1740

[8] Uda T, Serizawa M, San-nami T, Miyahara S. Prediction of formation of oriented lakes. Proc. 34th ICCE, ASCE. 2014. pp. 1-12

[9] Scheffers AM, Kelletat DH. Lakes of the World with Google Earth: Understanding our Environment. Coastal Research Library, Vol. 16. Switzerland: Springer International Publishing; 2016. p. 293

[10] Miyahara S, Uda T, Serizawa M, San-nami T. Prediction of effects of artificial alteration on segmentation of a slender water body. Coastal Sediments '15. 2015;**164**:1-14

[11] Wilson BW. Numerical prediction of ocean waves in the North Atlantic for December, 1959. Deut. Hydrogr. Zeit, Jahrgang 18, Heft 3. 1965. pp. 114-130

[12] Goda Y. Revisiting Wilson's formulas for simplified wind-wave prediction, Journal of Waterway. Port, Coastal and Ocean Engineering. 2003;**129**(2):93-95

[13] Serizawa M, Uda T, Miyahara S. Segmentation of water body given probability of occurrence of wind direction by circular or elliptic distribution. Proc. 35th Conf. Coastal Eng., sediment. 6. 2016. pp. 1-15

[14] San-nami T, Uda T, Gibo M, Ishikawa T, Miyahara S, Serizawa M. Change in carbonate beach triggered by construction of a bridge on Irabu Island and its simulation using BG model. Asian and Pacific Coasts 2013, Proc. 7th International Conf. 2013. pp. 24-31

[15] Seppälä M. Wind as a Geomorphic Agent in Cold Climates. New York: Cambridge University Press; 2004. p. 358